KCI CONRETE JOURNAL
Vol.14 No.1, March 2002, pp.15-22

Shrinkage-Induced Stresses at Early Ages in Composite Concrete Beams

Dong-Uk Choi [1)*] **and Chang-Ho Lee** [1)]

[1)] *Assistant Professor, Dept. of Architectural Engineering, Hankyong National University, Korea*

(Received September 24, 2001; Accepted December 17, 2001)

Abstract

Stresses that develop due to differential shrinkage between polymer modified cement mortar (PM) and Portland cement concrete (PCC) in a repaired concrete beam at early ages were investigated. Interface delamination or debonding of the newly cast repair material from the base is often observed in the field when the drying shrinkage of the repair material is relatively large. This study presents results of both experimental and analytical works. In the experimental part of the study, development of the material properties such as compressive strength, elastic modulus, interface bond strength, creep constant, and drying shrinkage was investigated by testing cylinders and beams for a three-week period in a constant-temperature chamber. Development of shrinkage-induced strains in a PM-PCC composite beam was determined. In the analytical part of the study, two analytical solutions were used to compare the experimental results with the analytically predicted values. One analysis method was of an exact type but could not consider the effect of creep. The other analysis method was rather approximate in nature but the creep effect was included. Comparison between the analytical and the experimental results showed that both analytical procedures resulted in stresses that were in fair agreement with the experimentally determined values. It may be important to consider the creep effect to estimate shrinkage-induced stresses at early ages.

Keywords: polymer modified cement mortar, repair, composite beam, interface shear stress, drying shrinkage, delamination.

1. Introduction

Polymer modified cement mortar (PM) is often used to repair or strengthen existing reinforced concrete beams, columns, or slabs. Drying shrinkage of the PM or coefficient of thermal expansion of the PM that is higher than that of the Portland cement concrete (PCC) can develop internal stresses that may be large enough to initiate delamination of the repair material from the base. Performance and integrity of a repaired structural member can be severely affected as a result of delamination. Chen et al. assuming linear elastic material properties proposed a closed form solution for the thermally-induced stress problems.[1)] While the thermally-induced stresses develop from a mismatch in the coefficient of thermal expansion (α) between the two different materials, stresses can also develop due to a differential shrinkage (i.e. shrinkage difference between the newly cast repair material and the existing base). The shrinkage-induced stresses can be analyzed in a similar way to the thermal stress analysis as the amount of the differential shrinkage can replace the mismatch of thermal coefficients of the two materials multiplied by the temperature change. It is noted, however, that most drying shrinkage develops at early ages and creep effect may play an important role. Silfwerbrand recently proposed an analytical procedure for the shrinkage-induced stress problems where a creep constant was used to include the creep effect.[2)] The objective of this study was to investigate the shrinkage-induced internal stresses in a composite concrete beam both analytically and experimentally as follows:

(1) Fabricate a PM-PCC composite beam and directly measure shrinkage-induced shear stress close to the interface of the beam;
(2) Perform analyses using two analytical methods (i.e. an exact method by Chen et al. and the method proposed by Silfwerbrand) and compare the analytical solutions with the experimental data;

* *Corresponding author*
Tel.: +82-031-670-5272; Fax.: +82-031-670-5015
E-mail address: choidu@hnu.hankyong.ac.kr

(3) Assess the importance of considering the creep effect in determining the shrinkage-induced stresses at early ages.

It needs to be noted that experimental data have rarely been published where an attempt was made to directly measure the shrinkage-induced stresses in repaired or strengthened reinforced concrete members using polymer modified cement mortar.[3,4]

2. Analytical procedures for shrinkage-induced stresses

Fig. 1 shows a composite beam where a relatively thin layer of a repair material (top layer) is placed on existing concrete (base beam). Because the two materials are fully bonded at the interface, the free shrinkage of the newly cast repair material is restricted by the bonded interface. As a result, the beam is subjected to flexure and the relatively thin top layer is primarily subjected to tensile stresses in the beam's axial direction. The magnitude of axial stress (σ_x) can be determined using elementary beam theory.[5-7] The axial stress has to vanish at the beam end as no external forces are acting at the end. Shear stress (τ_{xy}) and tensile or compressive stress acting in a direction normal to the interface (σ_y) develop toward the beam end. The distribution and magnitude of τ_{xy} and σ_y cannot be determined using elementary beam theory.

Chen et al.,[1] in an analysis of laminated wood beams subjected to temperature changes, formulated a two-dimensional elasticity problem by considering the compatibility conditions between the layers and the stress-free boundary conditions. Variational energy method was used to obtain a set of governing differential equations that satisfies stress-free boundary conditions. Analytical procedure proposed by Chen et al. provides an exact solution as far as the elastic material properties (i.e. E, v, and α) of the top and bottom layers remain the same and the beam is subjected to a uniform temperature change. Fig. 2 shows the internal stresses developed along the interface of a PM-PCC composite beam of Fig. 1 subjected to a uniform temperature drop of 10 °C determined using the Chen's method. The beam dimensions and the material properties used for the numerical evaluation of internal stresses plotted in Figs. 1 and 2 are summarized in Appendix 1. Taking an advantage of symmetric stress distribution, only the beam right-hand half is shown. In Fig. 2, τ_{xy} and σ_y develop only toward the beam end. It is noted in Fig. 2 that τ_{xy} becomes maximum very close to the end and vanishes at the end since there are no external shear forces acting at the end. It is also noted that the sums of the positive and negative σ_y (+ and – areas under the curve) are the same. Silfwerbrand[2] also proposed an analytical procedure for determining shrinkage-induced stresses in overlaid beams. The model, developed based on beam theory, assumes linear elastic material properties. Force

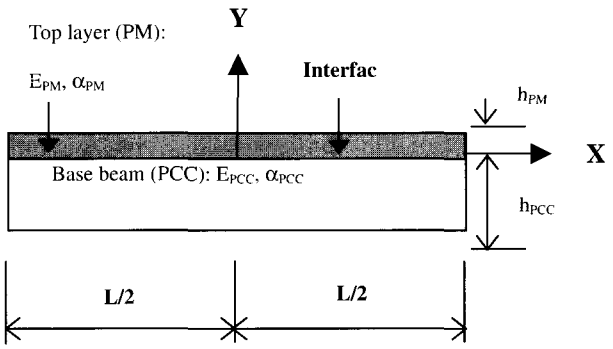

Fig. 1 A PM-PCC composite beam: $\alpha_{PM} > \alpha_{PCC}$

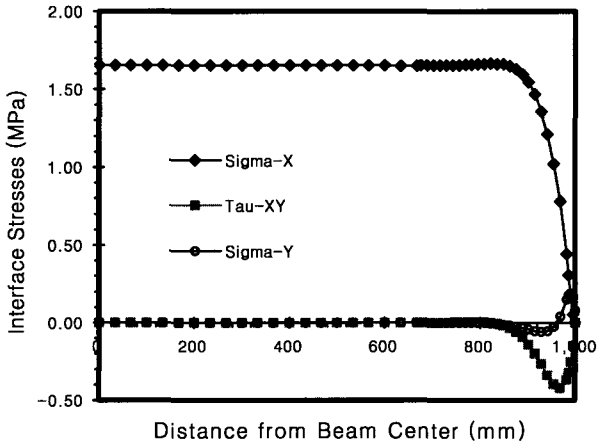

Fig. 2 Thermally-induced interface stresses in a PM-PCC composite beam:[1] σ_x = axial stress developed at the interface in the top layer (PM), τ_{xy}, σ_y = stresses developed at the interface, ΔT = -10°C

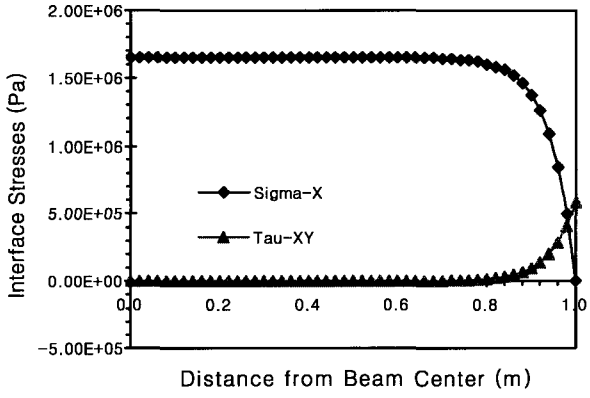

Fig. 3 Shrinkage-induced literface stresses in a PM-PCC composite beam:[2] σ_x = axial stress developed at the interface in the top layer (PM), τ_{xy} = interface shear stress, $\varepsilon_{sh} = (\alpha_{PCC} - \alpha_{PM}) * (\Delta T)$

equilibrium and a linear relationship between slip and shear stress at the interface are used to determine three unknown functions for the strains in the top and bottom layers, respectively, and the beam curvature. Axial strains and stresses in the beam and the interface shear stress can be determined using the proposed method. Two constants need to be experimentally determined prior to applying this analytical procedure: a creep constant (ϕ) and a constant (K) relating the shear stress and the slip between the top and bottom layers. Once two constants are determined, the shrinkage-induced stresses can be evaluated as shown in Fig. 3 for the same beam of Fig. 1.

The amount of the differential shrinkage (ε_{sh}) in Fig. 3 is the same as the product of the mismatch of thermal coefficients of the two materials multiplied by the temperature change ($\Delta\alpha * \Delta T$) in Fig. 2. By comparing the distribution and magnitude of stresses shown in Figs. 2 and 3, it is revealed that (1) σ_x is the same in both analytical procedure, (2) τ_{xy} is not the same, and (3) τ_{xy} does not become zero at the end in Fig. 3 because of approximate nature of the suggested analytical procedure by Silfwerbrand.

3. Experimentally-determined shrinkage-induced stresses

3.1 Preparation for test

3.1.1 Beam fabrication

Two PM-PCC composite beams (see Fig. 4) were fabricated for test as follows:

(1) Approximately one-year-old existing prestressed-concrete beams, 0.16m (W) x 0.20m (H) x 2.0m (L) each, were used as the base beam.

(2) Top surfaces of the base beams were roughened using hydroblasting to an extent that the coarse aggregates were lightly exposed.

(3) A thin layer (thickness = 20 mm) of polymer modified cement mortar was placed on the dry roughened surface.

(4) One beam was used to monitor the development of shrinkage-induced strains. The other beam was used to determine bond strengths at the interface.

It was assumed that the one-year-old base beam that contained two 12.7-mm diameter seven-wire prestressing strands would experience a negligible amount of drying shrinkage when compared to that of the newly cast PM for a relatively short three-week testing period. Mix proportions of the latex-modified PM are summarized in Table 1. Both beams were moved into a constant-temperature chamber where the temperature was set at 15+/- 1°C immediately after casting the top layer and wet-cured for 24 hours. One beam was instrumented using strain gages and strain rosettes as shown in Fig. 4. The purpose was to monitor strains developed in the beam due to drying shrinkage of the PM. As shown in Fig. 4(b) and (c), three 30-mm strain gages were installed on top surface of the PM at the beam center to measure axial strains. A total of six three-element strain rosettes was installed to measure shear strains developed close to the interface in the PM. The centroid of the 10-mm strain rosettes was 6 mm above the interface. Three, each, were installed on both

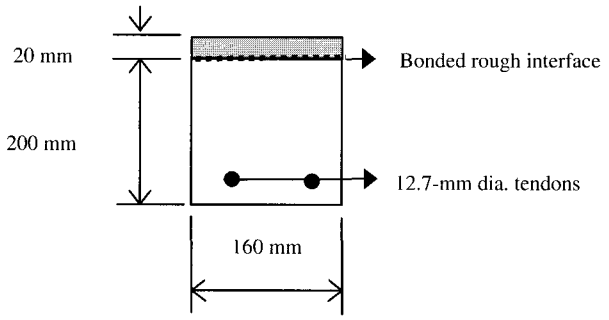

(a) Cross section

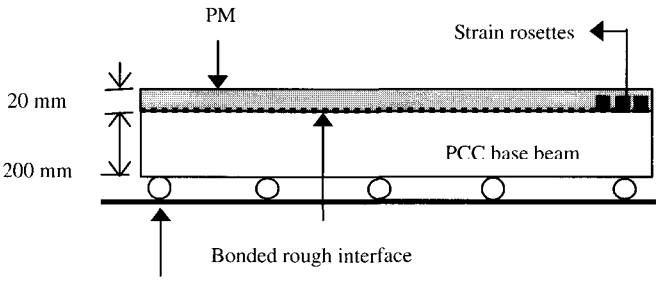

(b) Beam elevation

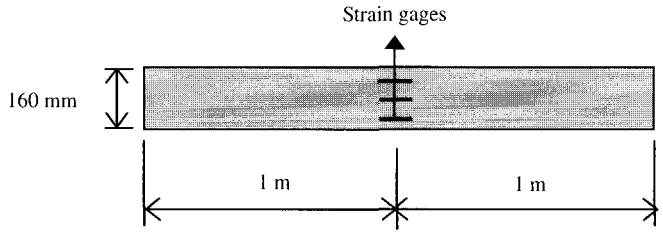

(c) View from the top

Fig. 4 Geometry of composite beam and instrumentation for strain measurement

Table 1 Mix proportions of PM, % by wt.

Part A	Cement	Admixture	Fine aggr.	Coarse aggr.[1)]
	8.6	11.4	40.0	40.0
Part B	Water	Polymer emulsion	Additive	
	63.8	34.4	1.8	

Note 1: Maximum coarse aggregate size = 5 mm,
2: Part A / Part B = 1 / 0.105 by wt.

side faces of the PM at distances 30 mm, 60 mm, and 150 mm away from the beam end.

3.1.2 Free shrinkage and creep constant

Concrete cylinders (∅100 mm x 200 mm) were used to determine compressive strengths and elastic moduli of the PM at 1, 4, 7, and 21 days after casting. Two concrete cylinders, each with a pair of 30-mm strain gages, were used for measuring the free shrinkage and the creep constant. All concrete cylinders were wet-cured for 24 hours and placed in the same constant-temperature chamber as the beams. For the creep test, a compressive load was increased successively in equal increments of $\Delta\sigma$ = 5MPa at 1 and 4 days. A creep constant ϕ was computed using the following equation.[2)]

$$\phi = \frac{\varepsilon_{tot} - \varepsilon_{sh} - \varepsilon_{el}}{\varepsilon_{el}} \quad (1)$$

$$\varepsilon_{el} = \sigma / E_c \quad (2)$$

where, ε_{tot}, ε_{sh}, ε_{el} are total strain of a loaded cylinder, free shrinkage of an unloaded cylinder, and elastic strain, respectively in Eq. 1. In addition, σ and E_c are compressive stress and elastic modulus, respectively, in Eq. 2.

3.1.3 Interface bond strength

As mentioned previously, one of two beams was used to determine the interface bond strengths. Masonry saw was used to cut short beams out from a 2-m-long beam that were subjected to direct shear test 21 days after casting. A constant (K) that relates the shear stress and the slip between the top and bottom layers in the analytical method suggested by Silfwerbrand was determined in the direct shear test. The tensile bond strength was determined after 21 days.

3.1.4 Data acquisition

A 30-channel TDS 303 data logger was used to digitally record the electronic signals from the strain gages and strain rosettes. A total of 26 channels was utilized: 3 for the strain gages installed on the top extreme fiber of the PM, 18 for the strain rosettes, 4 for two pairs of strain gages installed on concrete cylinders, and 1 for the thermo couple. The data acquisition started approximately 24 hours after casting the top layer immediately following the installation of strain gages and strain rosettes on the beam and cylinders. The rate of sampling was one data set per an hour for the test that lasted for 21 days.

3.2 Test results

3.2.1 Strength development

Compressive strengths, elastic moduli, Poisson's ratios are summarized in Tables 2 and 3. Cores obtained from the base beam were used to determine the compressive strength and elastic modulus of the base concrete. The compressive strengths were 25.5 MPa and 34.3 MPa for PM and PCC, respectively, by the time the experimental program was completed (21 days). The shear and tensile bond strengths at the interface were determined after 21 days with results summarized in Table 4. The average interface shear strength was 1.12 MPa while the average tensile bond strength at the interface was 3.29 MPa.

Table 2 Compressive strength development, MPa

Materials	1 day	4 days	7 days	21 days
PM[1]	21.6	22.7	25.3	25.5
Base concrete	34.3			

Note: 14-day compressive strength is interpolated to be 25.4 MPa

Table 3 Elastic modulus, MPa, and poisson's ratio

Materials		1 day	4 days	7 days	21 days
PM1	E	15,520	18,330	21,260	23,710
	ν[2]	--	--	--	0.20
Base concrete	E	39,500			
	ν	0.18			

Note 1: Elastic modulus after 14 days is interpolated to be 22,485 MPa, 2: Poisson's Ratio

Table 4 Bond strengths at interface after 21 days, MPa

Direct shear			Tensile
Replicate no.	τ_{max}	failed at	(12 tests)
1	0.95	interface	
2	1.17	ditto	average = 3.29
3	1.13	ditto	min. = 2.40
4	1.24	ditto	max. = 4.08
Average	1.12		

3.2.2 Development of shrinkage-induced strains

Fig. 5 shows the development of unrestrained drying shrinkage of the PM (free shrinkage) determined from a cylinder. It must be noted that the relative humidity could not be controlled in the constant-temperature chamber and, unfortunately, the effect of varying relative humidity is included in the curve as shown in Fig. 5. The relative humidity was high during the test period and ranged typically between 80% and 95% that may explain the relatively small amount of free shrinkage measured. The minimum value is -137 x 10^{-6} m/m about 15 days after casting in Fig. 5. Fig. 6 shows the creep test results. The creep test was performed to determine a creep constant that was used in the analytical procedure by Silfwerbrand. The creep constant is used to determine reduced elastic modulus (or shear modulus) as shown in Eqs. A-1 through A-6 of

Appendix 2.

Fig. 7 shows readings from the strain gages installed on top extreme fiber of the PM over time. Axial strains that developed in the PM were determined as the differences between the strain values shown in Fig. 7 and the free shrinkage measured from a cylinder shown in Fig. 5. Theory predicts that the shear strains will develop only toward the end of the composite beam which is shown in Fig. 8 where relatively large shear strains developed toward the end over time. It is noted in Fig. 8 that the sign of the shear strains determined at 150-mm distance from end is opposite of those determined at 30 and 60 mm. Although the theory assumes the bonded interface, actual roughness of the contact surface is not modeled and this sign reversal was considered as local phenomena. The absolute strain values seem to be more important. The absolute shear strains determined after 4 and 14 days are shown in Fig. 9 that clearly shows the localized concentration of the developed shear strains (or stresses) which are confined to a narrow region close to the beam end as predicted by theory.

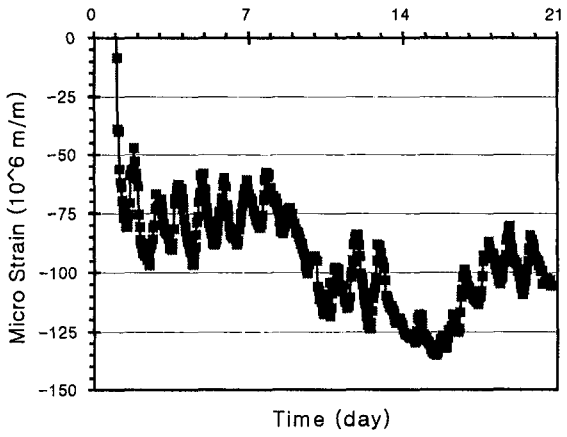

Fig. 5 Development of free shrinkage vs. time

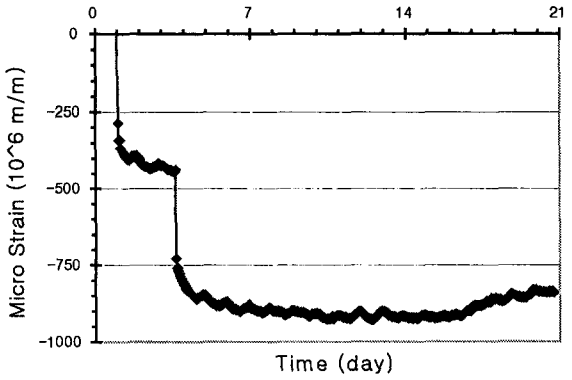

Fig. 6 Creep test results

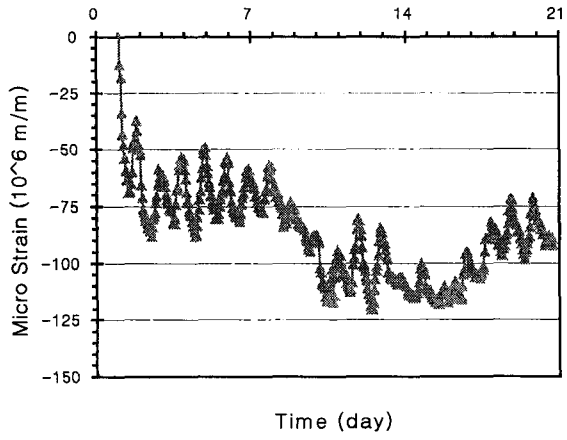

Fig. 7 Strain readings on top extreme fiber of PM

4. Analysis results

Two sets of experimental data determined at 4 and 14 days after the casting the top layer were selectively compared with analytical solutions. Numerical data used for analyses are summarized in Appendix 2.

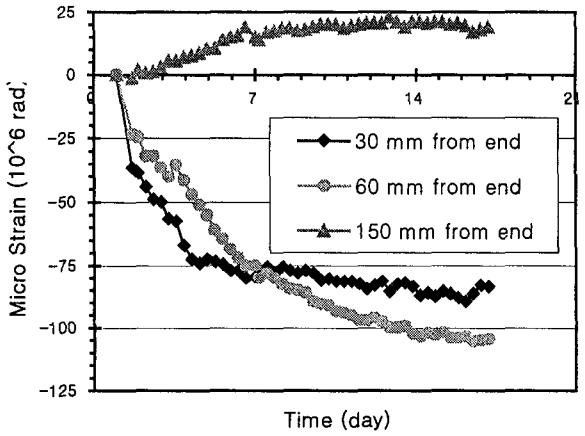

Fig. 8 Development of shear strains close to beam end

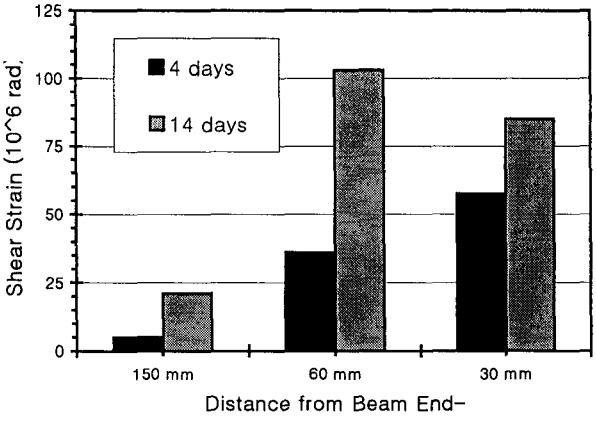

Fig. 9 Development of shear strains close to beam end after 4 and 14 days

4.1 Analytical solution by Silfwerbrand

Plots representing distribution of axial strains developed on top extreme fiber of the PM after 4 and 14 days are shown in Figs. 10 and 11, respectively. The experimentally determined axial strains seem to agree well with the theoretically predicted values as shown. In Figs. 12 and 13, shear stresses determined both experimentally and analytically are compared. Shear stresses from test were determined by multiplying the reduced shear modulus of the PM (see Eqs. A-1 through A-6 in Appendix 2) multiplied by the measured shear strains. The reduced shear moduli were used to include creep effect considered in the analytical method proposed by Silfwerbrand. The peak values match reasonably well between the test data and the analytical results as shown in Figs. 12 and 13. It must be noted that, while the analytically determined shear stresses are those at the interface, the experimentally determined shear stresses were based on strain readings measured 6 *mm* above the interface. The shear strains at the interface are expected to be higher.

Although the peak values seem to match reasonably well between the test data and the analytical results determined using the analytical method suggested by Silfwerbrand as shown in Figs. 12 and 13, this analytical method, however, should be applied with caution. As mentioned previously, the K constant that relates the interface shear stress and the slip between the top and bottom layers at the interface needs to be experimentally determined prior to applying this method. The interface shear stress is then found by multiplying K to the slip between the two layers. In this study, the K value was determined to be 1.12 x 10^{11} N/m^3 during the direct shear test. It must be noted that care should be taken in assessing this constant, because (1) the stress (or strain) gradient toward the beam end is directly proportional to this constant and (2) it was found to be rather difficult to experimentally determine K unless very sensitive gages were used.

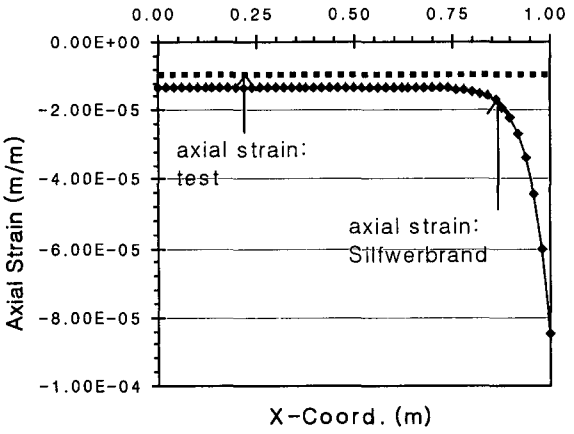

Fig. 10 Axial strain on top extreme fiber after 4 days: Silfwerbrand vs. test

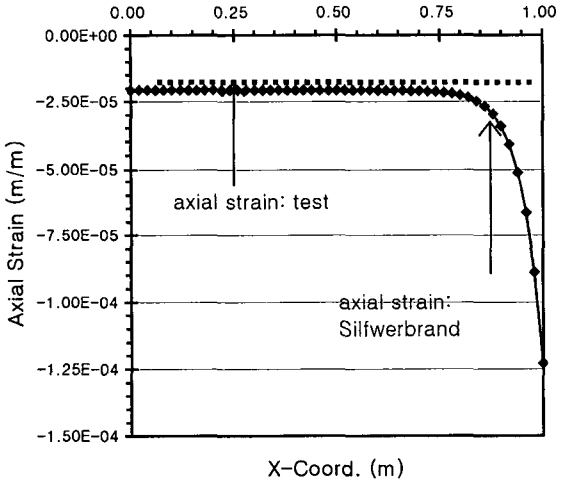

Fig. 11 Axial strain on top extreme fiber after 14 days: Silfwerbrand vs. test

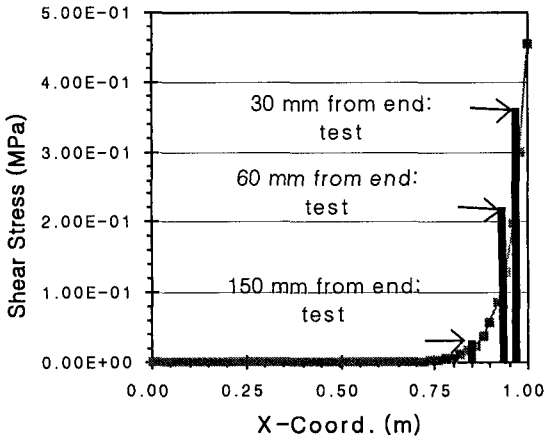

Fig. 12 Interface shear stress after 4 days: Silfwerbrand vs. test

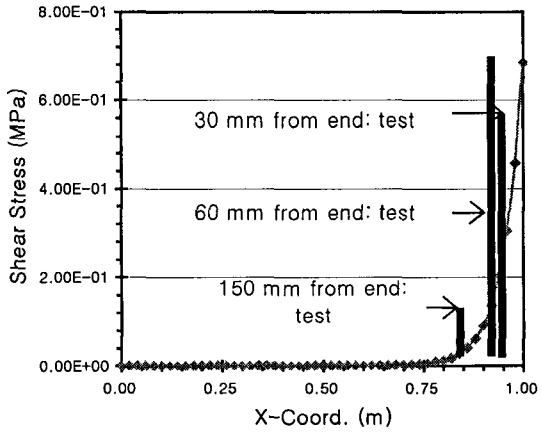

Fig. 13 Interfae shear stress after 14 days: Silfwerbrand vs. test

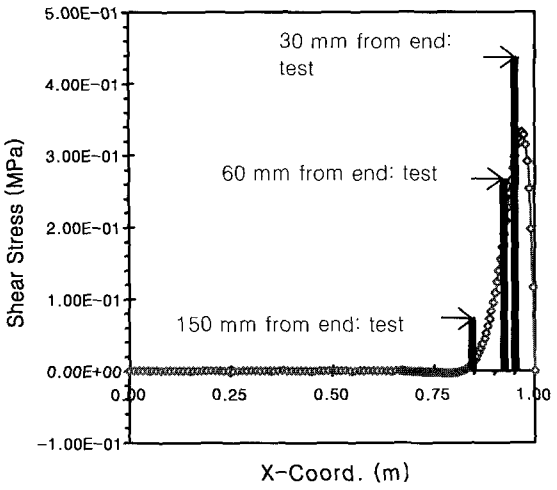

Fig. 14 Interface shear stress after 4 days: Chen et al. vs. test

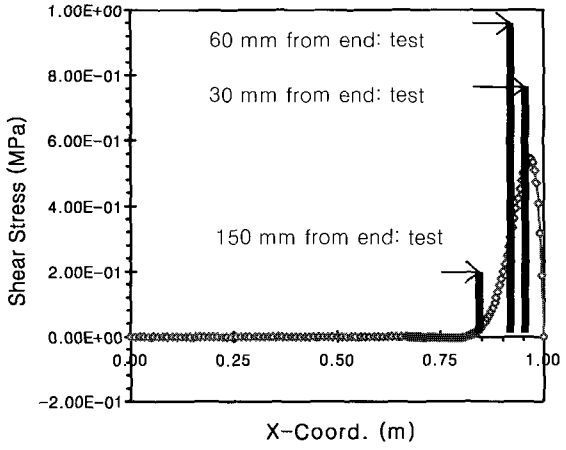

Fig. 15 Interface shear stress after 14 days: Chen et al. vs. test

4.2 Analytical solution by Chen et al.

In Figs. 14 and 15, experimentally determined shear stresses are compared to those determined analytically using Chen et al.'s analytical procedure. Shear stresses from test as shown in Figs. 14 and 15 were determined by multiplying unmodified shear modulus of the PM times the measured shear strains. Experimentally determined values are higher than those predicted by analysis using Chen et al.'s method as shown. The experimentally determined values are higher probably because the creep effect was not considered (i.e. the reduced shear modulus was not used). It is noted that, while the average interface shear strength determined by direct shear test was 1.12 MPa, the shear strength was 0.95 MPa at least in one test as shown in Table 4 that is close to the peak shear stress at 60 mm from end in Fig. 15. Considering the fact that no delaminations were observed in the test beam, the use of unmodified shear modulus probably resulted in overestimated stresses.

5. Conclusions

The objective of this study was to investigate the shrinkage-induced stresses developed in a composite concrete beam both analytically and experimentally. Comparison between the analytical and the experimental results revealed the following:

(1) Internal stresses were developed due to differential shrinkage;

(2) Experimentally determined axial strains agreed well with the theoretically predicted values;

(3) Experimental results showed the localized concentration of the shear strains (or stresses) development of which is confined to a narrow region close to the beam end as predicted by theory;

(4) Two analytical procedures used in this study resulted in shear stress distributions that are in fair agreement with the experimentally determined values;

(5) It may be important to consider the creep effect to estimate shrinkage-induced stresses at early ages.

ACKNOWLEDGEMENTS

Authors appreciate financial support for this study provided by Hankyong National University. It is also acknowledged that Reform System Co., Ltd. supplied the polymer modified cement mortar used in this study.

REFERENCES

1. Chen, D., Cheng, S., and Gerhardt, T.D., "Thermal Stresses in Laminated Beams," *Journal of Thermal Stresses*, Vol. 5, No. 1, 1982, pp. 67-84.
2. Silfwerbrand, J., "Stresses and Strains in Composite Concrete Beams Subjected to Differential Shrinkage," *ACI Structural Journal*, Vol. 94, No. 4, Jul.-Aug., 1997, pp. 347-353.
3. Choi, D.-U., Fowler, D.W., and Wheat, D.L., "Thermal Stresses in Polymer Concrete Overlays," *Properties and Uses of Polymers in Concrete*, ACI Special Publication SP166, 1996, pp. 93-122.
4. Al-Negheimish, A.I., "*Bond Strength, Long Term Performance and Temperature Induced Stresses in Polymer Concrete - Portland Cement Concrete Composite Members*," Ph.D. Dissertation, The University of Texas at Austin, 1988.
5. Timoshenko, S., "Analysis of Bi-Metal Thermostats," Journal of Strain Analysis, Vol. 11, 1926, pp. 233-255.
6. Birkland, H.W., "Differential Shrinkage in Composite Beams," *Journal of The American Concrete Institute*, Vol. 56, No. 11, 1960, pp. 1123-1136.

7. Zuk, W., "Thermal and Shrinkage Stresses in Composite Beams," *Journal of The American Concrete Institute*, Vol. 58, No. 3, 1961, pp. 327-337.

Appendix 1

Table A Beam dimensions used for analyses

Layer	Height, mm	Length, mm	Width
PM	20	2,000	unit width
PCC	200	2,000	ditto

Table B Material properties used for analyses

Material	E, MPa	ν	α, mm/mm/°C
PM	$2.0 * 10^4$	0.20	$20.0 * 10^{-6}$
PCC	$4.0 * 10^4$	0.18	$10.0 * 10^{-6}$

$$\varepsilon_{sh} = (\alpha_{PCC} - \alpha_{PM})*(\Delta T) = 100*10^{-6}\, m/m$$

Appendix 2

After 4 days

E_{PM} = 18,330 MPa; E_{PCC} = 39,500 MPa; h_{PM} = 20 mm; h_{PCC} = 200 mm; ν_{PM} = 0.2; ν_{PCC} = 0.18; L = 2.0 m; e_{sh} = 85 x 10^{-6} m/m

After 14 days

E_{PM} = 22,485 MPa; e_{sh} = 123 x 10^{-6} m/m

Additional data used for analytical method by Silfwerbrand after 4 days

$K = 1.12*10^{11}$ N/m^3

$$\phi_{PM} = \frac{\varepsilon_{tot} - \varepsilon_{sh} - \varepsilon_{el}}{\varepsilon_{el}} = \frac{440 - 85 - 290}{290} = 0.224 \quad \text{(A-1)}$$

$$E_1 = \frac{E_{PM}}{1+\phi_{PM}} = \frac{18{,}330}{1+0.224} = 14{,}975 \text{ MPa} \quad \text{(A-2)}$$

$$G_1 = \frac{E_1}{2(1+\nu)} = \frac{14{,}975}{2(1+0.2)} = 6{,}240 \text{ MPa} \quad \text{(A-3)}$$

$$E_2 = \frac{E_{PCC}}{1+\phi_{PCC}}(1-\rho_2) + E_s\rho_2 = 40{,}373 \text{ MPa}$$

Additional data used for analytical method by Silfwerbrand after 14 days

$$\phi_{PM} = \frac{\varepsilon_{tot} - \varepsilon_{sh} - \varepsilon_{el}}{\varepsilon_{el}} = \frac{920 - 123 - 580}{580} = 0.374 \quad \text{(A-4)}$$

$$E_1 = \frac{E_{PM}}{1+\phi_{PM}} = \frac{22{,}485}{1+0.374} = 16{,}365 \text{ MPa} \quad \text{(A-5)}$$

$$G_1 = \frac{E_1}{2(1+\nu)} = \frac{16{,}365}{2(1+0.2)} = 6{,}819 \text{ MPa} \quad \text{(A-6)}$$